

# Molecular dynamics studies of horse prion protein wild type and its S167D mutant

Jiapu Zhang

*Centre of Informatics and Applied Optimisation, The Federation University Australia, Ballarat, Victoria, Australia  
j.zhang@federation.edu.au; jiapu\_zhang@hotmail.com* Centre of Informatics and Applied Optimisation, The Federation  
University Australia, Mount Helen Campus, Mount Helen, Ballarat, Victoria 3353, Australia

**Abstract:** Prion diseases or called transmissible spongiform encephalopathies (TSEs) are fatal neurodegenerative diseases characterised by the accumulation of an abnormal prion protein isoform (PrP<sup>Sc</sup>: rich in  $\beta$ -sheets - about 30%  $\alpha$ -helix and 43%  $\beta$ -sheet), which is converted from the normal prion protein (PrP<sup>C</sup>: predominant in  $\alpha$ -helix - about 42%  $\alpha$ -helix and 3%  $\beta$ -sheet). However, prion disease has not been reported in horses up to now; therefore, horses are known to be a species resistant to prion diseases. Residue S167 in horse has been cited as critical protective residue for encoding PrP conformational stability in prion-resistance. According to the “protein-only” hypothesis, PrP<sup>Sc</sup> is responsible for both spongiform degeneration of the brain and disease transmissibility. Thus, understanding the conformational dynamics of PrP<sup>Sc</sup> from PrP<sup>C</sup> is key to developing effective therapies. This article is to do molecular dynamics studies on the horse PrP wild-type and its S167D mutant to understand their conformational dynamics; interesting results will be discussed.

**Key words:** Horse prion protein; protective residue S167; S167D mutant; molecular dynamics studies; secrets of resisting prion diseases.

## Introduction

Prion diseases are incurable neurodegenerative diseases caused by aberrant conformations of the prion protein (PrP). Many animals develop similar diseases, but rabbits, dogs, and horses show unusual resistance to prion diseases [1-15]. This resistance could be due to protective changes in the sequence of the corresponding PrP in each animal. Structural studies have identified S174, S167, and D159 as the key protective residues in rabbit, horse, and dog PrP, respectively [1-15]. But no systemic molecular dynamics (MD) studies currently support the protective activity of these residues, especially for horse PrP residue S167. Experimental laboratory results revealed that expression of horse PrP-S167D (which carries substitution for the equivalent residue in hamster (the species being susceptible to prion diseases) PrP) shows high toxicity in behavioural and anatomical assays [14]. Thus, this article aims to MD study horse PrP wild-type (WT) NMR structure 2KU4.pdb and S167D-mutant (Mutant) homology structure (constructed by this article). We will present in this article useful protective bioinformatics of S167 and discuss the structural features that make horse PrP more stable. The findings of this article might contribute to the development of drugs/compounds that stabilize PrP structure and prevent the formation of toxic conformations of prion diseases.

## Materials and Methods

The material is same as the one of [13]: the NMR structure 2KU4.pdb of horse PrP WT (119-231). Basing on 2KU4.pdb, we just make one mutation S167D only at position 167 from hamster PrP residue ASP167 and get a homology structure for S167D-mutant of horse PrP.

For both the WT and the Mutant, the low pH in the MD simulations is achieved by the change of residues HIS, ASP, GLU into HIP, ASH, GLH respectively and the Cl<sup>-</sup> ions added by the XLEaP module of

AMBER package, and the neutral pH in the MD simulations is achieved by the change of residues HIS into HID and the Na<sup>+</sup> ions added by the XLEaP module of AMBER package.

The MD simulations are done at 300 K, 350 K and 450 K respectively as Section 1.2 of [16] described.

## Results and Discussions

For convenience, we give some acronyms. For WT horse normal cellular prion protein [12] (horse PrP<sup>C</sup> with PDB entry 2KU4), its structural region GLY119-SER231 consists of  $\beta$ -strand 1 ( $\beta$ 1: MET129-ALA133),  $\alpha$ -helix 1 ( $\alpha$ 1: ASP144-ARG151),  $3_{10}$ -helix 1 ( $3_{10}$ H1: MET154-ARG156),  $\beta$ -strand 2 ( $\beta$ 2: GLN160-TYR163),  $3_{10}$ -helix 2 ( $3_{10}$ H2: VAL166-GLU168),  $\alpha$ -helix 2 ( $\alpha$ 2: GLN172-THR192),  $\alpha$ -helix 3 ( $\alpha$ 3: GLU200-ARG228), and the loops linking them each other. As we all know, the stability of a protein is maintained by its salt bridges, hydrogen bonds, hydrophobic contacts, van der Waals contacts and disulfide bonds (for PrP monomer there exists a disulfide bond (S-S) between CYS179 and CYS214) etc. to drive to be able to perform the biological function of the protein; we denote SBs, HBs, HYDs, vdWs for salt bridges, hydrogen bonds, hydrophobic interactions, and van der Waals contacts respectively. We denote amino acids (or residues) as 'aa'. Residue 167 is in the  $\beta$ 2- $\alpha$ 2 loop of PrPs, and both Syrian hamsters and horses have a well-defined and highly ordered  $\beta$ 2- $\alpha$ 2 loop.

Firstly, we optimized the WT and Mutant structures and their backbone atoms RMSD (root mean square deviation) value is 0.495090 angstroms. We find the mutation made that (i) *for the secondary structures* in the segment TYR169-ASN171 (before the N-terminal of  $\alpha$ 2) Turn is changed into Coil, in the segment LYS194-GLU196 (next to the C-terminal of  $\alpha$ 2) Coil is changed into Turn, and extend the C-terminal  $\alpha$ 1 from Bend-Turn structure in the segment GLU152-ASN153; (ii) *for the SBs* ASP147-ARG148 (in  $\alpha$ 1), ASP147-ARG151 (in  $\alpha$ 1), ASP178-HIS177 (in  $\alpha$ 2), ASP202-ARG156 (linking  $\alpha$ 3 -  $3_{10}$ H1), GLU152-ARG151 (linking  $\alpha$ 1- $3_{10}$ H1-loop -  $\alpha$ 1), GLU168-ARG164 (linking  $3_{10}$ H2 -  $\beta$ 2- $3_{10}$ H2-loop), GLU200-LYS204 (in  $\alpha$ 3), GLU211-ARG208 (in  $\alpha$ 3), GLU221-LYS220 (in  $\alpha$ 3) (except for ASP144-ARG148 (in  $\alpha$ 1), GLU196-ARG156 (linking  $\alpha$ 2- $\alpha$ 3-loop -  $3_{10}$ H1)) disappeared in the Mutant, (iii) *for the HBs* 12 HBs are less than in WT (see details in Table 1), and (iv) *for the  $\pi$ -interactions*  $\pi$ -cations PHE141-ARG208.NH2<sup>+</sup> (linking  $\beta$ 1- $\alpha$ 1-loop -  $\alpha$ 3), HIS177-LYS173.NZ<sup>+</sup> (in  $\alpha$ 2) disappeared in the Mutant. Residue 167 is in the  $\beta$ 2- $\alpha$ 2-loop and the mutation S167D results in increased negative charges on the surface around the  $\beta$ 2- $\alpha$ 2-loop region (ASP is a negatively charged residue).

**Table 1. The S167D mutation made changes in the network of hydrogen bonds (HBs):**

<i>HBs kept</i>	<i>locations</i>	<i>HBs lost</i>	<i>locations</i>
ARG228.N-ALA224.O	in $\alpha$ 3	TYR149.OH-ASP202.OD1	$\alpha$ 1 - $\alpha$ 3
ASN181.N-HIS177.O	in $\alpha$ 2	ASN153.ND2-TYR149.O	$\alpha$ 1- $3_{10}$ H1-loop - $\alpha$ 1
CYS179.N-PHE175.O	in $\alpha$ 2	ARG156.N-ASN153.O	$3_{10}$ H1 - $\alpha$ 1- $3_{10}$ H1-loop
CYS214.N-VAL210.O	in $\alpha$ 3	ARG164.NE-GLU168.OE2	$\beta$ 2- $3_{10}$ H2-loop - $3_{10}$ H2
GLN217.N-MET213.O	in $\alpha$ 3	ARG164.NH2-GLU168.OE1	$\beta$ 2- $3_{10}$ H2-loop - $3_{10}$ H2
GLU207.N-VAL203.O	in $\alpha$ 3	HIS177.ND1-ASP178.OD1	in $\alpha$ 2
GLU211.N-GLU207.O	in $\alpha$ 3	ASP178.N-ASN174.O	in $\alpha$ 2
GLU221.N-GLN217.O	in $\alpha$ 3	HIS187.N-THR183.O	in $\alpha$ 2
GLY131.N-VAL161.O	$\beta$ 1 - $\beta$ 2	THR192.N-THR188.O	in $\alpha$ 2
HIS177.N-LYS173.O	in $\alpha$ 2	LYS194.N-THR191.O	$\alpha$ 2- $\alpha$ 3-loop - $\alpha$ 2
ILE182.N-ASP178.O	in $\alpha$ 2	GLU196.N-THR191.OG1	$\alpha$ 2- $\alpha$ 3-loop - $\alpha$ 2
ILE205.N-THR201.O	in $\alpha$ 3	PHE198.N-THR192.OG1	$\alpha$ 2- $\alpha$ 3-loop - $\alpha$ 2
ILE215.N-GLU211.O	in $\alpha$ 3	GLN212.NE2-GLU211.OE2	in $\alpha$ 3
LYS185.N-ASN181.O	in $\alpha$ 2	GLN217.NE2-TYR163.OH	in $\alpha$ 3
LYS204.N-GLU200.O	in $\alpha$ 3	GLN219.NE2-ILE215.O	in $\alpha$ 3

MET129.N-TYR163.O	$\beta 1 - \beta 2$	GLN227.NE2-GLU223.O	in $\alpha 3$
MET134.N-ASN159.O	$\beta 1 - \alpha 1 - \text{loop} - 3_{10}\text{H1} - \beta 2 - \text{loop}$	SER231.OG-GLN227.O	C-terminal - $\alpha 3$
MET206.N-ASP202.O	in $\alpha 3$		
MET213.N-VAL209.O	in $\alpha 3$	<b>new HBs</b>	<b>locations</b>
PHE225.N-GLU221.O	in $\alpha 3$	TYR150.N-GLU146.O	in $\alpha 1$
THR183.OG1-CYS179.O	in $\alpha 2$	ARG151.N-ASP147.O	in $\alpha 1$
THR188.N-VAL184.O	in $\alpha 2$	GLU152.N-ARG148.O	$\alpha 1 - 3_{10}\text{H1} - \text{loop} - \alpha 1$
THR190.N-GLN186.O	in $\alpha 2$	ASN171.ND2-ASN174.OD1	$3_{10}\text{H2} - \alpha 2 - \text{loop} - \alpha 2$
THR216.N-GLN212.O	in $\alpha 3$	GLN186.N-ILE182.O	in $\alpha 2$
TYR149.N-TYR145.O	in $\alpha 1$		
TYR150.OH-PRO137.O	$\alpha 1 - \beta 1 - \alpha 1 - \text{loop}$		
TYR162.N-THR183.OG1	$\beta 2 - \alpha 2$		
TYR218.N-CYS214.O	in $\alpha 3$		
TYR222.N-TYR218.O	in $\alpha 3$		
VAL176.N-GLN172.O	in $\alpha 2$		
VAL180.N-VAL176.O	in $\alpha 2$		
VAL184.N-VAL180.O	in $\alpha 2$		
VAL189.N-LYS185.O	in $\alpha 2$		
VAL203.N-THR199.O	$\alpha 3 - \alpha 2 - \alpha 3 - \text{loop}$		
VAL209.N-ILE205.O	in $\alpha 3$		
VAL210.N-MET206.O	in $\alpha 3$		

Because the S167D mutation made some HBs & SBs in  $\alpha 2$  &  $\alpha 3$  and some  $\pi$ -cations lost, we may see *the molecular structure of the Mutant (compared with the WT) is unstable especially in the regions of  $\alpha 2$  &  $\alpha 3$  (especially at both terminals of  $\alpha 2$ )*. On the contrary, in Section 4.1 of [16], the MD results show that *the N-terminal half of  $\alpha 1$  is not stable at 350 K and 450 K, but the  $\beta 2 - \alpha 2 - \text{loop}$  has less variations than other PrP loops* being due to the well-defined and highly ordered  $\beta 2 - \alpha 2 - \text{loop}$  structure of horse PrP. These imply to us that the S167D mutation reversed the MD results of [16] – S167 is critical to contribution of horse PrP<sup>C</sup> structure stability.

The above is just a snapshot's results of WT or Mutant. Next, let us study 30ns' MD results of WT and Mutant.

We first consider the secondary structure developments (Table 2 and Figures 1-3), HBs (Table 3), SBs (Table 4), and HYDs (Tables 5-6) results of 30ns' MD of WT.

**Table 2. Secondary Structures percentages of the WT at 300K, 350 K, 450 K during 30 ns' MD simulations (seed1, seed2, seed3) in neutral and low pH environments:**

			B $\beta$ -bridge	G $3_{10}$ -helix	I $\pi$ -helix	H $\alpha$ -helix	E $\beta$ -sheet	T Turn	S Bend
300 K	Low pH	Seed1	0.00%	4.88%	0.00%	50.41%	3.54%	7.79%	7.65%
		Seed2	0.26%	3.32%	0.09%	48.54%	4.63%	8.34%	9.00%
		Seed3	0.21%	4.44%	0.00%	46.63%	4.07%	8.93%	10.89%
Neutral pH		Seed1	0.00%	4.53%	0.00%	51.20%	3.54%	5.04%	8.73%
		Seed2	0.13%	3.94%	0.03%	50.15%	3.55%	9.00%	7.94%
		Seed3	0.50%	2.90%	0.00%	51.17%	3.73%	8.34%	8.83%
350 K	Low pH	Seed1	0.21%	2.85%	0.00%	49.39%	3.42%	8.34%	10.18%
		Seed2	0.34%	3.55%	0.03%	48.73%	4.11%	9.05%	9.11%
		Seed3	0.37%	3.24%	0.00%	49.29%	4.14%	8.67%	8.20%
Neutral pH		Seed1	0.47%	4.90%	0.00%	46.79%	4.96%	9.62%	7.92%
		Seed2	0.18%	3.60%	0.03%	49.18%	3.49%	9.04%	9.60%
		Seed3	0.67%	4.70%	0.03%	49.53%	4.31%	6.76%	9.19%
450 K	Low pH	Seed1	1.09%	3.47%	0.09%	42.18%	1.17%	12.46%	12.70%
		Seed2	0.93%	4.85%	0.12%	41.37%	3.60%	14.31%	12.84%
		Seed3	0.76%	4.25%	0.06%	38.34%	3.14%	14.80%	15.43%

	Neutral pH	Seed1	0.81%	4.35%	0.00%	38.38%	0.64%	16.43%	14.61%
		Seed2	0.73%	4.09%	0.12%	42.47%	3.33%	11.43%	14.64%
		Seed3	0.28%	4.07%	0.09%	45.13%	4.05%	10.64%	7.31%

Table 2 shows us compared with under neutral pH environment (i) at 300 K H  $\alpha$ -helices become less and E  $\beta$ -strands become more under low pH environment; (ii) at 350 K G  $3_{10}$ -helices become less, for seed3 I  $\pi$ -helices become less, for seed2 & seed3 H  $\alpha$ -helices become less, and for seed2 E  $\beta$ -strands become more under low pH environment; and (iii) at 450 K B  $\beta$ -bridges become more, for seed1 G  $3_{10}$ -helices become less, for seed3 I  $\pi$ -helices become less, for seed2 & seed3 H  $\alpha$ -helices become less, and for seed1 & seed2 E  $\beta$ -strands become more under low pH environment. From Table 2, we can see the PrP<sup>C</sup> is predominant in  $\alpha$ -helix - at least 38.34%  $\alpha$ -helix, under neutral pH environment the percentages of  $\alpha$ -helix become less and less as the temperatures go up from 300 K to 350 K and to 450 K, however under low pH environment this rule is not obeyed for seed2 & seed3 from 300 K to 350 K. PrP<sup>C</sup> has  $\beta$ -sheet structure about 3%, and at 300 K the change from neutral pH environment to low pH environment makes the percentages of  $\beta$ -sheet increase (Table 2).

In Figure 1 we notice that at 300 K (i) under neutral pH environment, for seed2 during 0-11.8 ns the  $\alpha 2$  C-terminal segment aa 189-195 and for seed1 & seed3 the  $\alpha 3$  N-terminal segment aa 200-201 are in Turn structure; and (ii) under low pH environment, for seed2 during 0-9.4 ns segment aa 160-161 is extension of  $\beta 1$  sheet structure and for seed3 the  $\alpha 3$  C-terminal segment 220-226 is in Turn structure.

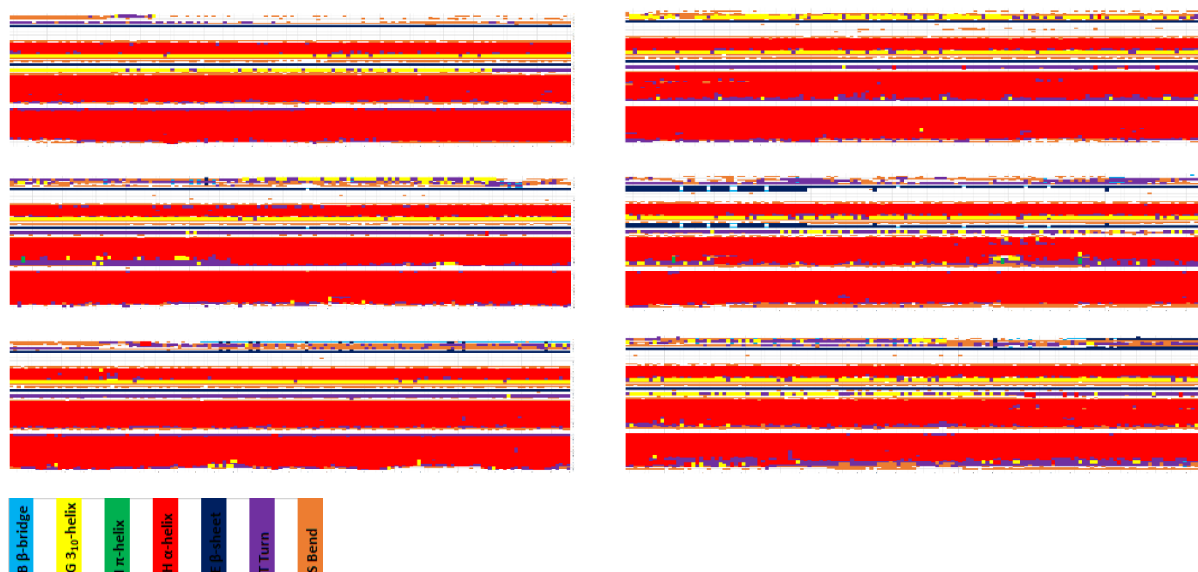


**Figure 1. Secondary Structures of the WT at 300 K during 30 ns' MD simulations (left: neutral pH environment, right: low pH environment; up to down: seed1, seed2, seed3).**

In Figure 2 we notice that at 350 K under neutral pH environment for seed1 (i)  $\beta 1$  E  $\beta$ -strand structure extends to segment aa 120-130 and (ii)  $\alpha 1$  H  $\alpha$ -helix structure unfolds in segment aa 152-157 during 13-30 ns.

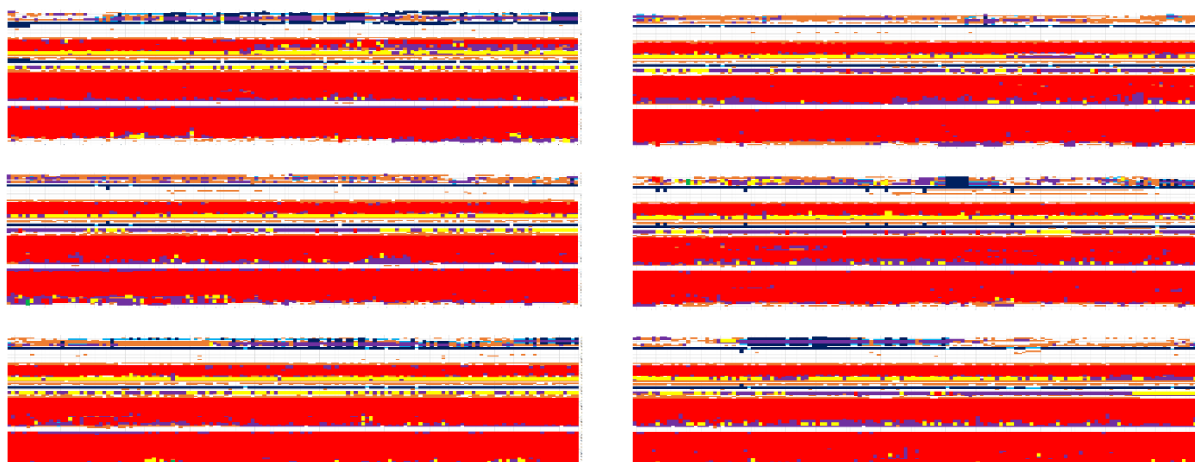


**Figure 2. Secondary Structures of the WT at 350 K during 30 ns' MD simulations (left: neutral pH environment, right: low pH environment; up to down: seed1, seed2, seed3).**

In Figure 3 we notice that at 450 K (i) under neutral pH environment, for seed1 the E  $\beta$ -sheet's two  $\beta$ -strands are broken, for seed2 the  $\beta$ -sheet structure becomes into  $\beta$ -bridge structure during 9-17.4 ns, and for all seeds the N- and C-terminals of  $\alpha$ 1,  $\alpha$ 2,  $\alpha$ 3 are unfolding; and (ii) under low pH environment,  $\beta$ -sheet is broken for seed1, becomes into  $\beta$ -bridge for seed2, & is broken for seed3 from 18<sup>th</sup> ns, and for seed3  $\alpha$ 1 is unfolding from 20.6<sup>th</sup> ns,  $\alpha$ 2 is unfolding from 26.6<sup>th</sup> ns - we should also notice the RMSD values steadily go up under low pH environment at 450K (Fig. 4.9a of [16]).

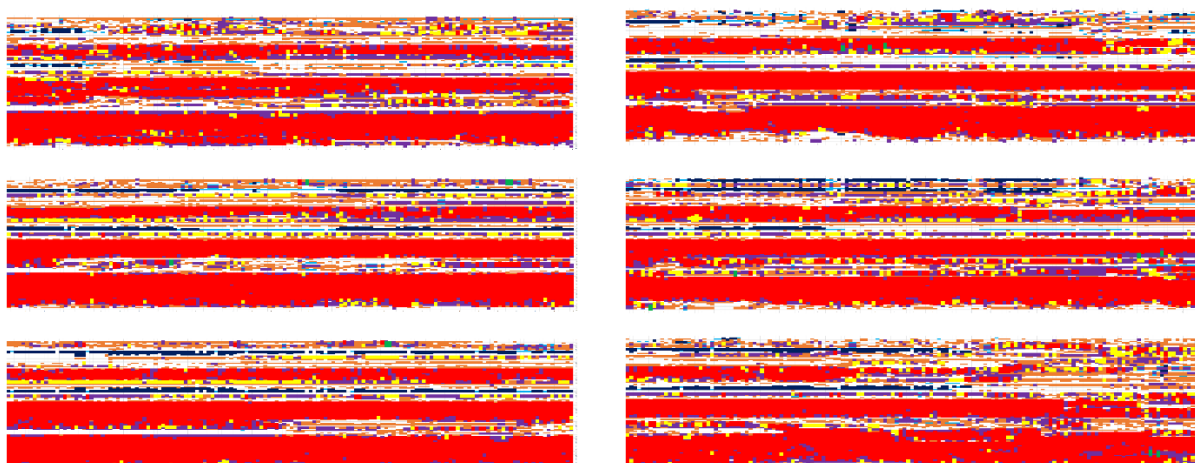


**Figure 3. Secondary Structures of the WT at 450 K during 30 ns' MD simulations (left: neutral pH environment, right: low pH environment; up to down: seed1, seed2, seed3).**

Generally, for WT, the above Secondary Structures results (shown in Table 2 and Figures 1-3), in combination with the RMSD (root mean square deviation), Radius of Gyration, RMSF (RMS fluctuation), B-factor results in Section 4.1 of [16], show us that at 450 K under low pH environment (compared with under neutral pH environment)  $\alpha$ -helices start to unfold and  $\beta$ -strands/bridges become more.

Let us do analyses on HBs, SBs, and HYDs of WT. Under low pH environment at MD-production constant temperatures of 300 K, 350 K and 450 K, all the HBs in Table 3 were removed. Under neutral

pH environment at the temperature levels 300 K, 350 K and 450 K, the HBs ASP202-ARG<sup>+</sup>156/TYR157/TYR149 and ASP178-ARG<sup>+</sup>164/TYR128/TYR169 are always existing (Table 3). Here we should denote that there exists a HB ASP178@O-TYR128@OH.HH 11.81 for seed1 at 350 K under low pH environment. In addition, in Table 3 the following HBs are also contributing to the structural stability of WT under neutral pH environment: GLU146-LYS<sup>+</sup>204 & GLN172-GLN219 at 300 K, GLU196-ARG<sup>+</sup>156 & GLU221-TYR163 & PRO158-ARG<sup>+</sup>136 at 350 K, and GLU196-GLY119/SER120 & GLU221-SER167 & LEU138-TYR150 & GLY126/GLY127-ARG<sup>+</sup>164 & GLY131-GLN160 & GLU146-ARG<sup>+</sup>208 at 450 K.

**Table 3. All HBs (with % occupied rates >10% for seed1, seed2 and seed3) of WT at 300 K, 350 K and 450 K under neutral pH environment during the whole 3 sets of 30 ns' MD simulations for each temperature level.**

HBs at 300 K under neutral pH environment	HBs at 350 K under neutral pH environment	HBs at 450 K under neutral pH environment
ASP202@OD1-TYR157@OH.HH 29.19, 84.64, 44.75	GLU196@O-ARG <sup>+</sup> 156@NE.HE 10.27, 12.50, 0	ASP202@OD1-ARG <sup>+</sup> 156@NE.HE 0, 0, 11.57
ASP202@OD2-TYR157@OH.HH 62.79, 0, 49.53	GLU196@O-ARG <sup>+</sup> 156@NH1.HH12 0, 0, 17.27	ASP202@OD1-ARG <sup>+</sup> 156@NH1.HH12 23.27, 28.72, 14.80
ASP202@OD1-ARG <sup>+</sup> 156@NH1.HH11 0, 67.38, 0	GLU196@O-ARG <sup>+</sup> 156@NH2.HH21 21.24, 0, 0	ASP202@OD1-ARG <sup>+</sup> 156@NH2.HH21 0, 5.00, 14.12
ASP202@OD1-ARG <sup>+</sup> 156@NH1.HH12 60.02, 0, 42.64	GLU196@O-ARG <sup>+</sup> 156@NH2.HH22 0, 0, 12.43	ASP202@OD1-ARG <sup>+</sup> 156@NH2.HH22 16.40, 20.87, 16.53
ASP202@OD2-ARG <sup>+</sup> 156@NH1.HH12 28.89, 0, 42.91	GLU196@OE1-ARG <sup>+</sup> 156@NH2.HH21 0, 17.91, 0	ASP202@OD2-ARG <sup>+</sup> 156@NE.HE 0, 0, 10.60
ASP202@OD1-ARG <sup>+</sup> 156@NH2.HH22 33.65, 0, 48.65	GLU196@OE2-ARG <sup>+</sup> 156@NE.HE 0, 10.62, 13.05	ASP202@OD2-ARG <sup>+</sup> 156@NH1.HH12 17.80, 22.15, 17.12
ASP202@OD2-ARG <sup>+</sup> 156@NH2.HH22 60.77, 0, 43.96	GLU196@OE2-ARG <sup>+</sup> 156@NH2.HH21 0, 0, 11.42	ASP202@OD2-ARG <sup>+</sup> 156@NH2.HH21 0, 0, 15.88
ASP202@OD1-TYR149@OH.HH 0, 12.02, 0	ASP202@OD1-TYR149@OH.HH 0, 19.46, 18.03	ASP202@OD2-ARG <sup>+</sup> 156@NH2.HH22 21.58, 27.68, 13.57
ASP202@OD2-TYR149@OH.HH 0, 67.42, 0	ASP202@OD2-TYR149@OH.HH 0, 22.37, 41.93	ASP202@OD1-TYR157@OH.HH 0, 20.78, 32.18
ASP178@OD2-TYR128@OH.HH 27.04, 0, 0	ASP202@OD1-ARG <sup>+</sup> 156@NE.HE 0, 0, 10.28	ASP202@OD2-TYR157@OH.HH 0, 22.68, 29.00
ASP178@OD1-TYR128@OH.HH 25.90, 0, 12.08	ASP202@OD1-ARG <sup>+</sup> 156@NH1.HH11 0, 0, 45.58	ASP202@OD1-TYR149@OH.HH 0, 7.25, 10.40
ASP178@OD2-ARG <sup>+</sup> 164@NH2.HH21 0, 82.87, 40.21	ASP202@OD1-ARG <sup>+</sup> 156@NH1.HH12 49.23, 24.93, 0	GLU196@OE1-GLY119@N.H1 10.47, 0, 0
ASP178@OD1-ARG <sup>+</sup> 164@NE.HE 0, 61.45, 30.03	ASP202@OD1-ARG <sup>+</sup> 156@NH2.HH21 0, 0, 10.11	GLU196@OE1-SER120@OG.HG 12.35, 0, 0
ASP178@OD1-ARG <sup>+</sup> 164@NH2.HH21 0, 22.19, 30.73	ASP202@OD1-ARG <sup>+</sup> 156@NH2.HH22 31.87, 28.07, 0	ASP178@OD1-ARG <sup>+</sup> 164@NE.HE 0, 11.82, 8.88
ASP178@OD2-ARG <sup>+</sup> 164@NE.HE 0, 0, 13.35	ASP202@OD2-ARG <sup>+</sup> 156@NH1.HH11 0, 20.97, 0	ASP178@OD1-ARG <sup>+</sup> 164@NH1.HH11 0, 0, 18.53
GLU146@OE1-LYS <sup>+</sup> 204@NZ.HZ1 0, 16.53, 0	ASP202@OD2-ARG <sup>+</sup> 156@NH1.HH12 28.89, 26.21, 0	ASP178@OD1-ARG <sup>+</sup> 164@NH1.HH12 11.90, 0, 0
GLU146@OE2-LYS <sup>+</sup> 204@NZ.HZ1 0, 16.10, 0	ASP202@OD2-ARG <sup>+</sup> 156@NH2.HH21 0, 0, 14.52	ASP178@OD1-ARG <sup>+</sup> 164@NH2.HH21 0, 17.60, 12.73
GLU146@OE2-LYS <sup>+</sup> 204@NZ.HZ2 0, 16.09, 0	ASP202@OD2-ARG <sup>+</sup> 156@NH2.HH22 45.29, 18.65, 0	ASP178@OD2-ARG <sup>+</sup> 164@NH1.HH11 0, 0, 16.20
GLU146@OE1-LYS <sup>+</sup> 204@NZ.HZ2 0, 15.53, 0	ASP202@OD1-TYR157@OH.HH 43.71, 27.18, 66.71	ASP178@OD2-ARG <sup>+</sup> 164@NH1.HH12 10.07, 0, 0
GLU146@OE1-LYS <sup>+</sup> 204@NZ.HZ3 0, 17.57, 0	ASP202@OD2-TYR157@OH.HH 30.47, 57.38, 0	ASP178@OD2-ARG <sup>+</sup> 164@NH2.HH21 7.88, 18.63, 13.17
GLU146@OE2-LYS <sup>+</sup> 204@NZ.HZ3 0, 17.39, 0	ASP178@OD1-ARG <sup>+</sup> 164@NE.HE 13.48, 23.84, 15.06	ASP178@OD1-TYR169@OH.HH 0, 27.60, 15.75
GLN172@OE1-GLN219@NE2.HE21 10.89, 0, 0	ASP178@OD1-ARG <sup>+</sup> 164@NH2.HH21 24.08, 15.08, 23.03	ASP178@OD2-TYR169@OH.HH 0, 24.72, 17.75
ASP178OD1-TYR169@HH 35.55, 0, 0	ASP178@OD2-ARG <sup>+</sup> 164@NE.HE 36.29, 0, 0	ASP178@OD1-TYR128@OH.HH 0, 12.25, 6.50
ASP178OD2-TYR169@HH 40.47, 0, 0	ASP178@OD2-ARG <sup>+</sup> 164@NH2.HH21 30.03, 23.94, 20.27	ASP178@OD2-TYR128@OH.HH 0, 12.47, 5.90
	ASP178@OD1-TYR169@OH.HH 32.27, 25.65, 57.75	GLU221@OE1-SER167@OG.HG 11.70, 0, 0
	ASP178@OD2-TYR169@OH.HH 0, 11.96, 30.44	GLU221@OE2-SER167@OG.HG 10.38, 0, 0
	GLU221@OE1-TYR163@OH.HH 23.40, 0, 26.15	LEU138@O-TYR150@OH.HH 0, 10.75, 0
	GLU221@OE2-TYR163@OH.HH 24.55, 14.65, 25.87	GLY126@O-ARG <sup>+</sup> 164@NH2.HH21 0, 0, 15.48
	PRO158@O-ARG <sup>+</sup> 136@NE.HE 0, 10.81, 0	GLY127@O-ARG <sup>+</sup> 164@NE.HE 0, 0, 14.48
	ASP178@OD1-TYR128@OH.HH 6.19, 35.51, 50.43	GLY131@O-GLN160@NE2.HE21 0, 0, 13.70
	ASP178@OD2-TYR128@OH.HH 5.35, 22.53, 38.97	GLU146@OE1-ARG <sup>+</sup> 208@NE.HE 0, 0, 11.57
		GLU146@OE1-ARG <sup>+</sup> 208@NH2.HH21 5.88, 5.28, 11.72
		GLU146@OE2-ARG <sup>+</sup> 208@NH2.HH21 5.18, 0, 13.53

Table 4 lists all the SBs (with occupancy rates >5%) of the WT under neutral pH environment at 30 ns' MD-production constant temperatures of 300 K, 350 K and 450 K. All the SBs of 300 K (ASP144-ARG<sup>+</sup>148, ASP147-HID<sup>+</sup>140/ARG<sup>+</sup>148/ARG<sup>+</sup>151, HID177-LYS<sup>+</sup>173, ASP178-ARG<sup>+</sup>164, HID187-ARG<sup>+</sup>156, GLU152-ARG<sup>+</sup>148/ARG<sup>+</sup>151, GLU168-ARG<sup>+</sup>164, GLU196-ARG<sup>+</sup>156/LYS<sup>+</sup>194, ASP202-ARG<sup>+</sup>156, GLU207-LYS<sup>+</sup>204/ARG<sup>+</sup>208, GLU221-HID<sup>+</sup>177/ARG<sup>+</sup>208/LYS<sup>+</sup>220, GLU223-LYS<sup>+</sup>220) are still existing at 350 K and 450 K. In addition, at 350 K there are additional SBs GLU223@CD-ARG<sup>+</sup>228@CA.CZ & HID187@CG-ARG<sup>+</sup>156@CA.CZ & ASP144@CG-HID<sup>+</sup>140@ND1.HD1, and at 450 K there are additional

SBs GLU146@CD-ARG+208@CA.CZ, HID187@CG-LYS+185@CA.NZ, GLU152@CD-ARG+156@CA.CZ, HID187@NE2-LYS+185@CA.NZ, GLU146@CD-HID+140@ND1.HD1, ASP144@CG-HID+140@ND1.HD1, HID140@NE2-ARG+136@CA.CZ, ASP202@CG-LYS+194@CA.NZ, GLU168@CD-ARG+228@CA.CZ, GLU200@CD-HID+187@ND1.HD1, GLU146@CD-LYS+204@CA.NZ, HID140@NE2-ARG+208@CA.CZ, HID140@CG-ARG+136@CA.CZ, GLU200@CD-LYS+194@CA.NZ, GLU221@CD-ARG+228@CA.CZ, GLU207@CD-HID+177@ND1.HD1. From Tables 3-4 we may know the *polar contacts* ASP178-ARG+164, ASP202-ARG+156 (weaker), GLU196-ARG+156, GLU146-ARG+208 (strong only at 450 K) contribute to the structural stability of WT during the MD simulations. The positions of the *special SBs* [HID187-ARG+156 (linking  $\alpha 2$  and  $3_{10}H1$ ), GLU211-HID+177 (linking  $\alpha 3$  and  $\alpha 2$ )], the *special polar contacts* [ASP178-ARG+164 (linking  $\alpha 2$  and  $\beta 2-3_{10}H2$ -loop), ASP202-ARG+156 (linking  $\alpha 3$  and  $3_{10}H1$ ), GLU196-ARG+156 (linking  $\alpha 2$ - $\alpha 3$ -loop and  $3_{10}H1$ ), GLU146-ARG+208 (linking  $\alpha 1$  and  $\alpha 3$ )], and the *SBs* [GLU223-LYS+220, GLU207-LYS+204/ARG+208, GLU211-ARG+208/LYS+220, GLU223-LYS+220 being within  $\alpha 3$ , HID177-LYS+173 being within  $\alpha 2$ , ASP144-ARG+148, ASP147-ARG+148/ARG+151 being within  $\alpha 1$ , GLU196-LYS+194 being within the  $\alpha 2$ - $\alpha 3$ -loop, GLU152-ARG+148/ARG+151 linking the  $\alpha 1$ - $3_{10}H1$ -loop with  $\alpha 1$ , GLU168-ARG+164 linking the  $\beta 2-3_{10}H2$ -loop and  $3_{10}H2$ , ASP147-HID+140 linking  $\alpha 1$  and the  $\beta 1$ - $\alpha 1$ -loop] should be noticed.

**Table 4. SBs (with occupancy rate >5%) of the WT during 3 sets of 30 ns' MD simulations under neutral pH environment at 300 K, 350 K, 450 K (from left to right in turns: 300K seed1-seed3, 350 K seed1-seed3, 450 K seed1-seed3):**

SBs at 300 K under neutral pH environment	SBs at 350 K under neutral pH environment	SBs at 450 K under neutral pH environment
ASP147@CG-ARG+148@CA.CZ 100, 100, 100	ASP147@CG-ARG+148@CA.CZ 100, 100, 100	ASP147@CG-ARG+148@CA.CZ 100, 100, 100
GLU211@CD-ARG+208@CA.CZ 99.99, 98.53, 99.88	GLU211@CD-ARG+208@CA.CZ 99.75, 99.49, 99.19	GLU211@CD-ARG+208@CA.CZ 98.50, 99.32, 97.43
GLU207@CD-LYS+204@CA.NZ 99.70, 92.81, 99.90	GLU207@CD-LYS+204@CA.NZ 99.58, 95.18, 94.64	GLU207@CD-LYS+204@CA.NZ 81.43, 95.43, 95.37
GLU221@CD-LYS+220@CA.NZ 99.18, 95.05, 99.53	GLU221@CD-LYS+220@CA.NZ 95.19, 75.51, 95.72	GLU152@CD-ARG+148@CA.CZ 79.35, 37.07, 30.50
GLU207@CD-ARG+208@CA.CZ 97.93, 89.95, 90.66	GLU223@CD-LYS+220@CA.NZ 84.79, 88.04, 89.61	GLU223@CD-LYS+220@CA.NZ 52.90, 84.60, 85.40
GLU223@CD-LYS+220@CA.NZ 83.49, 86.61, 84.31	HID177@CG-LYS+173@CA.NZ 89.28, 68.55, 83.69	GLU207@CD-ARG+208@CA.CZ 78.65, 77.78, 71.73
HID177@CG-LYS+173@CA.NZ 76.03, 54.27, 59.23	HID177@NE2-LYS+173@CA.NZ 84.88, 59.56, 79.02	GLU152@CD-ARG+151@CA.CZ 64.87, 41.73, 48.42
ASP178@CG-ARG+164@CA.CZ 8.54, 80.97, 72.61	GLU207@CD-ARG+208@CA.CZ 82.31, 75.41, 70.49	GLU221@CD-LYS+220@CA.NZ 59.77, 67.45, 71.52
ASP144@CG-ARG+148@CA.CZ 56.94, 63.26, 81.40	ASP144@CG-ARG+148@CA.CZ 69.22, 66.07, 69.63	HID177@CG-LYS+173@CA.NZ 35.13, 61.08, 61.32
HID187@NE2-ARG+156@CA.CZ 75.33, 79.47, 78.88	GLU196@CD-LYS+194@CA.NZ 80.79, 46.75, 13.83	HID177@NE2-LYS+173@CA.NZ 24.10, 50.62, 48.95
HID177@NE2-LYS+173@CA.NZ 73.13, 44.92, 48.37	GLU152@CD-ARG+148@CA.CZ 19.88, 51.91, 50.99	ASP147@CG-HID+140@ND1.HD1 57.98, 56.63, 71.32
ASP147@CG-HID+140@ND1.HD1 32.85, 59.40, 5.03	HID187@NE2-ARG+156@CA.CZ 8.05, 50.02, 68.03	ASP147@CG-ARG+151@CA.CZ 53.13, 57.55, 52.87
GLU152@CD-ARG+148@CA.CZ 41.30, 57.81, 22.23	ASP147@CG-HID+140@ND1.HD1 66.73, 14.95, 50.97	ASP144@CG-ARG+148@CA.CZ 46.73, 40.42, 42.32
GLU152@CD-ARG+151@CA.CZ 40.62, 24.43, 46.85	ASP147@CG-ARG+151@CA.CZ 40.29, 51.06, 19.25	GLU168@CD-ARG+164@CA.CZ 18.28, 42.77, 9.27
ASP147@CG-ARG+151@CA.CZ 24.14, 6.27, 36.33	GLU168@CD-ARG+164@CA.CZ 38.75, 33.56, 57.47	GLU146@CD-ARG+208@CA.CZ 5.67, 19.18, 13.50
ASP178@CG-HID+177@ND1.HD1 5.60, 14.60, 21.83	GLU152@CD-ARG+151@CA.CZ 65.20, 42.93, 42.81	ASP178@CG-HID+177@ND1.HD1 16.07, 17.85, 19.48
GLU211@CD-HID+177@ND1.HD1 20.18, 8.37, 12.57	GLU196@CD-ARG+156@CA.CZ 17.17, 41.71, 43.47	GLU211@CD-HID+177@ND1.HD1 16.42, 16.27, 12.23
GLU196@CD-LYS+194@CA.NZ 0, 63.33, 0	GLU211@CD-HID+177@ND1.HD1 27.48, 15.45, 17.77	HID187@CG-LYS+185@CA.NZ 38.85, 5.92, 0
GLU168@CD-ARG+164@CA.CZ 52.00, 0, 8.60	ASP178@CG-HID+177@ND1.HD1 10.42, 14.12, 8.83	ASP178@CG-ARG+164@CA.CZ 0, 22.00, 38.58
GLU196@CD-ARG+156@CA.CZ 0, 9.63, 0	ASP178@CG-ARG+164@CA.CZ 10.45, 33.61, 0	GLU152@CD-ARG+156@CA.CZ 34.87, 0, 0
ASP202@CG-ARG+156@CA.CZ 0, 6.53, 0	GLU223@CD-ARG+228@CA.CZ 0, 0, 10.11	HID187@NE2-LYS+185@CA.NZ 25.88, 0, 0
	HID187@CG-ARG+156@CA.CZ 0, 0, 7.57	GLU196@CD-LYS+194@CA.NZ 0, 24.88, 14.97
	ASP202@CG-ARG+156@CA.CZ 0, 0, 6.69	HID187@NE2-ARG+156@CA.CZ 0, 15.08, 24.72
	ASP144@CG-HID+140@ND1.HD1 7.40, 0, 0	GLU146@CD-HID+140@ND1.HD1 24.42, 0, 16.37
		ASP144@CG-HID+140@ND1.HD1 0, 5.23, 19.77
		GLU196@CD-ARG+156@CA.CZ 0, 16.48, 16.42
		HID140@NE2-ARG+136@CA.CZ 14.30, 0, 0
		ASP202@CG-LYS+194@CA.NZ 0, 12.78, 14.15
		GLU168@CD-ARG+228@CA.CZ 9.57, 0, 0
		ASP202@CG-ARG+156@CA.CZ 9.35, 0, 0
		GLU200@CD-HID+187@ND1.HD1 8.30, 0, 0
		GLU146@CD-LYS+204@CA.NZ 0, 5.88, 5.47
		HID140@NE2-ARG+208@CA.CZ 0, 0, 11.40
		HID140@CG-ARG+136@CA.CZ 7.42, 0, 0
		GLU200@CD-LYS+194@CA.NZ 0, 0, 10.70
		GLU221@CD-ARG+228@CA.CZ 7.33, 0, 0

Table 5 lists the basic HYDs (with occupancy rate 100%) maintained all the time under low or neutral pH environments at 300 K or 350 K or 450 K – all these basic HYDs are always contributing to the structural stability of the WT.

**Table 5. HYDs (with occupancy rate 100%) of the WT at 300 K, 350 K, 450 K during 30 ns' MD simulations whether under low or neutral pH environments:**

<i>Under low pH environment</i>	<i>Under neutral pH environment</i>	<i>Position in the PrP structure</i>
PHE225@CB-ALA224@CA.C	PHE225@CB-ALA224@CA.C	Within $\alpha$ 3
ALA224@CB-PHE225@CA.C	ALA224@CB-PHE225@CA.C	Within $\alpha$ 3
VAL210@CB-VAL209@CA.C	VAL210@CB-VAL209@CA.C	Within $\alpha$ 3
VAL209@CB-VAL210@CA.C	VAL209@CB-VAL210@CA.C	Within $\alpha$ 3
VAL209@CB-MET206@CA.C	VAL209@CB-MET206@CA.C	Within $\alpha$ 3
MET206@CB-ILE205@CA.C	MET206@CB-ILE205@CA.C	Within $\alpha$ 3
ILE205@CB-MET206@CA.C	ILE205@CB-MET206@CA.C	Within $\alpha$ 3
VAL176@CB-PHE175@CA.C	VAL176@CB-PHE175@CA.C	Within $\alpha$ 2
PHE175@CB-VAL176@CA.C	PHE175@CB-VAL176@CA.C	Within $\alpha$ 2
VAL166@CB-PRO165@CA.C	VAL166@CB-PRO165@CA.C	Within $\beta$ 2- $\beta$ <sub>10</sub> H2-loop
PRO165@CB-VAL166@CA.C	PRO165@CB-VAL166@CA.C	Within $\beta$ 2- $\beta$ <sub>10</sub> H2-loop
ILE139@CB-LEU138@CA.C	ILE139@CB-LEU138@CA.C	Within $\beta$ 1- $\alpha$ 1-loop
LEU138@CB-ILE139@CA.C	LEU138@CB-ILE139@CA.C	Within $\beta$ 1- $\alpha$ 1-loop
LEU138@CB-PRO137@CA.C	LEU138@CB-PRO137@CA.C	Within $\beta$ 1- $\alpha$ 1-loop
PRO137@CB-LEU138@CA.C	PRO137@CB-LEU138@CA.C	Within $\beta$ 1- $\alpha$ 1-loop
MET134@CB-ALA133@CA.C	MET134@CB-ALA133@CA.C	Linking $\beta$ 1 and $\beta$ 1- $\alpha$ 1-loop
ALA133@CB-MET134@CA.C	ALA133@CB-MET134@CA.C	Linking $\beta$ 1 and $\beta$ 1- $\alpha$ 1-loop
LEU130@CB-MET129@CA.C	LEU130@CB-MET129@CA.C	Within $\beta$ 1
MET129@CB-LEU130@CA.C	MET129@CB-LEU130@CA.C	Within $\beta$ 1
VAL122@CB-VAL121@CA.C	VAL122@CB-VAL121@CA.C	Within N-terminal
VAL121@CB-VAL122@CA.C	VAL121@CB-VAL122@CA.C	Within N-terminal
MET213@CB-VAL210@CA.C 99.98, 100, 99.98	MET213@CB-VAL210@CA.C 99.97, 100, 100	Within $\alpha$ 3
MET206@CB-VAL203@CA.C 95.20, 100, 99.93	MET206@CB-VAL203@CA.C 100, 99.90, 100	Within $\alpha$ 3

For HYDs, we also find some special and important HYDs listed in Table 6, which disappeared under low pH environment (except for the HYD VAL210@CB-VAL180@CA.C at 300 K under low pH environment), and completely disappeared at higher temperature 450 K. From Table 6, we know that the HYD VAL176@CB-ILE215@CA.C contributes the stability at 300 K under neutral pH environment, the HYD VAL210@CB-VAL180@CA.C contributes the stability at 300 K under low pH environment, and HYDs VAL210@CB-VAL180@CA.C, MET213@CB-VAL161@CA.C, VAL161@CB-MET213@CA.C not only contribute to the stability under neutral pH environment at 300 K but also at 350 K. All these 100% HYDs disappeared at 450 K. Generally, we can see that low pH environment or/and higher temperature will make the protein structural stability become weaker.

**Table 6. Some special HYDs (almost with occupancy rate 100%) of the WT at 300 K and 350 K during 30 ns' MD simulations under neutral pH environment:**

<i>300 K – under neutral pH environment</i>	<i>350 K – under neutral pH environment</i>		<i>Position in the PrP structure</i>
VAL210@CB-VAL180@CA.C	VAL210@CB-VAL180@CA.C	100% Exist at 300 K - low pH	Linking $\alpha$ 3 and $\alpha$ 2
MET213@CB-VAL161@CA.C	MET213@CB-VAL161@CA.C		Linking $\alpha$ 3 and $\beta$ 2



VAL161@CB-MET213@CA.C	VAL161@CB-MET213@CA.C		Linking $\beta 2$ and $\alpha 3$
VAL176@CB-ILE215@CA.C			Linking $\alpha 2$ and $\alpha 3$

In summary, the molecular structure of the Mutant (compared with the WT) is unstable especially in the regions of  $\alpha 2$  &  $\alpha 3$  (especially at both terminals of  $\alpha 2$ ) and S167 is critical to the contribution of WT horse PrP<sup>C</sup> structure stability. The S167D mutation made the WT lost its (i) SBs such as ASP147-ARG148 (in  $\alpha 1$ ), ASP147-ARG151 (in  $\alpha 1$ ), ASP178-HIS177 (in  $\alpha 2$ ), ASP202-ARG156 (linking  $\alpha 3$  -  $3_{10}$ H1), GLU152-ARG151 (linking  $\alpha 1$ - $3_{10}$ H1-loop -  $\alpha 1$ ), GLU168-ARG164 (linking  $3_{10}$ H2 -  $\beta 2$ - $3_{10}$ H2-loop), GLU211-ARG208 (in  $\alpha 3$ ); (ii) an important polar contact ASP202-ARG<sup>+</sup>156; (iii) two  $\pi$ -cations PHE141-ARG208.NH2<sup>+</sup> (linking  $\beta 1$ - $\alpha 1$ -loop -  $\alpha 3$ ), HIS177-LYS173.NZ<sup>+</sup> (in  $\alpha 2$ ); (iv) one important HB GLU221-SER167; and redistributed the negative charges on the surface around the  $\beta 2$ - $\alpha 2$ -loop region so that the well-defined and highly ordered  $\beta 2$ - $\alpha 2$ -loop structure of WT horse PrP<sup>C</sup> has more variations in the Mutant. Our WT and Mutant MD results have confirmed that the single amino acid differences at position 167 might influence the overall protein structures of WT and Mutant.

### Concluding Remarks

In [12], we were told the NMR structure of horse PrP<sup>C</sup> at 25 degrees C contains a well-structured and highly structure-ordered  $\beta 2$ - $\alpha 2$ -loop, with  $\alpha 3$  this loop forms a binding site for a chaperone 'protein X', and within this loop the single amino acid S167 is unique to the PrP sequences of equine species. S167 was reported to be a protective residue for horse PrP<sup>C</sup>. Our secondary structure MD studies show to us two performances (i) *for the WT the N-terminal half of  $\alpha 1$  is not stable and the  $\beta 2$ - $\alpha 2$ -loop has less variations than other loops but* (ii) *for the Mutant (compared with the WT) is unstable in the regions of  $\alpha 2$  &  $\alpha 3$  (especially at both terminals of  $\alpha 2$ ) and in the binding site for 'protein X'.* Detailed HBs, SBs, HYDs bioinformatics to explain the reasons for the performances were presented from the analyses of our MD results.

### Acknowledgements

This research (with project no. pb04 at Federation University Australia and under NCI) was undertaken with the assistance of resources and services from the National Computational Infrastructure (NCI), which is supported by the Australian Government.

### Disclosure statement

No potential conflict of interest was reported by the authors.

### References

- [1] Vorberg I, Martin HG, Eberhard P, Suzette AP (2003) Multiple amino acid residues within the rabbit prion protein inhibit formation of its abnormal isoform. J Virol 77(3):2003–2009
- [2] Wen Y, Li J, Xiong MQ, Peng Y, Yao WM, Hong J, Lin DH (2010) Solution structure and dynamics of the I214V mutant of the rabbit prion protein. PLoS ONE 5(10):e13273

- [3] Wen Y, Li J, Yao WM, Xiong MQ, Hong J, Peng Y, Xiao GF, Lin DH (2010) Unique structural characteristics of the rabbit prion protein. *J Biol Chem* 285(41):31682–31693
- [4] Khan MQ, Sweeting B, Mulligan VK, Arslan PE, Cashman NR, Pai EF, Chakrabartty A (2010) Prion disease susceptibility is affected by  $\beta$ -structure folding propensity and local side-chain interactions in PrP. *Proc Natl Acad Sci USA* 107(46):19808–19813
- [5] Sweeting B, Brown E, Khan MQ, Chakrabartty A, Pai EF (2013) N-terminal helix-cap in  $\alpha$ -helix 2 modulates  $\beta$ -state misfolding in rabbit and hamster prion proteins. *PLoS ONE* 8(5):e63047
- [6] Polymenidou M, Trusheim H, Stallmach L, Moosa R, Julius JA, Mielea G, Lenzbauer C, Aguzzia A (2008) Canine MDCK cell lines are refractory to infection with human and mouse prions. *Vaccine* 26(21):2601–2614
- [7] Hasegawa K, Mohri S, Yokoyama T (2013) Comparison of the local structural stabilities of mammalian prion protein (PrP) by fragment molecular orbital calculations. *Prion* 7(2):185–191
- [8] Sanchez-Garcia J, Jensen K, Zhang Y, Rincon-Limas DE, Fernandez-Funez P (2016) A single amino acid (Asp159) from the dog prion protein suppresses the toxicity of the mouse prion protein in *Drosophila*. *Neurobiol Dis* 95:204–209
- [9] Fernández-Borges N, Parra B, Vidal E, Eraña H, Sánchez-Martín MA, de Castro J, Elezgarai SR, Pumarola M, Mayoral T, Castilla J (2017) Unraveling the key to the resistance of canids to prion diseases. *PLoS Pathog* 13(11):e1006716
- [10] Lysek DA, Schorn C, Nivon LG, Esteve-Moya V, Christen B, Calzolari L, von Schroetter C, Fiorito F, Herrmann T, Guntert P (2005) Prion protein NMR structures of cats, dogs, pigs, and sheep. *Proc Natl Acad Sci USA* 102(3):640–645
- [11] Zhang JP (2021) Molecular dynamics studies of dog prion protein wild-type and its D159N mutant. *J Biomol Struct Dyn* 39(12):4234-4242
- [12] Perez DR, Damberger FF, Wuthrich K (2010) Horse prion protein NMR structure and comparisons with related variants of the mouse prion protein. *J Mol Biol* 400(2):121-128
- [13] Zhang JP (2011) The structural stability of wild-type horse prion protein. *J Biomol Struct Dyn* 29(2):369-377
- [14] Fernández-Funez P (2021) The prion protein zoo: identification of protective residues from prion-resistant animals. <http://www.cajal.csic.es/actividades2017/2017-10-30-PedroFernandezSketch.pdf> (Accessed on 29/09/2021)
- [15] Myers RR, Sanchez-Garcia J, Leving DC, Fernandez-Funez P (2021) New *Drosophila* models to uncover the intrinsic and extrinsic factors mediating the toxicity of the human prion protein. bioRxiv preprint posted on 25/06/2021, doi: 10.1101/2021.06.24.449794
- [16] Zhang JP (2018) Structural dynamics analyses of prion protein structures - The resistance to prion diseases down under. Springer. ISBN 978-981-10-8814-8 (print), doi: 10.1007/978-981-10-8